



Simultaneous improvements of strength and toughness in topologically interlocked ceramics

Mohammad Mirkhalaf^a, Tao Zhou^a, and Francois Barthelat^{a,1}

^aDepartment of Mechanical Engineering, McGill University, Montreal, QC H3A 2K6, Canada

Edited by David A. Weitz, Harvard University, Cambridge, MA, and approved July 23, 2018 (received for review April 27, 2018)

Topologically interlocked materials (TIMs) are an emerging class of architected materials based on stiff building blocks of well-controlled geometries which can slide, rotate, or interlock collectively providing a wealth of tunable mechanisms, precise structural properties, and functionalities. TIMs are typically 10 times more impact resistant than their monolithic form, but this improvement usually comes at the expense of strength. Here we used 3D printing and replica casting to explore 15 designs of architected ceramic panels based on platonic shapes and their truncated versions. We tested the panels in quasi-static and impact conditions with stereomaging, image correlation, and 3D reconstruction to monitor the displacements and rotations of individual blocks. We report a design based on octahedral blocks which is not only tougher (50×) but also stronger (1.2×) than monolithic plates of the same material. This result suggests that there is no upper bound for strength and toughness in TIMs, unveiling their tremendous potential as structural and multifunctional materials. Based on our experiments, we propose a nondimensional “interlocking parameter” which could guide the exploration of future architected systems.

architected materials | topologically interlocked materials | bioinspiration | ceramics | impact loading

Specific microstructures, heterogeneities, or hybrid compositions are now widely used in modern materials to generate high performance (1). These concepts are now pushed to the extreme with architected materials, which contain highly controlled structures and morphological features at length scales intermediate between traditional microstructure and the whole component (2). These information-rich materials can be programmed with specific architectures, geometries, and interfaces to generate unusual and attractive combinations of properties and functionalities, for example negative Poisson’s ratio (3), unusually high stiffness (4, 5), or high toughness (6–9). Architected materials include the now well-studied lattice materials which contain only a small fraction of solid (10). In contrast, the less-studied dense architected materials are fully solid and are made of building blocks of well-defined size and shape, arranged in two or three dimensions (11, 12). The geometry and arrangement of the blocks can be designed to generate interlocking in “topologically interlocked materials” (TIMs) without the need for adhesive or mortar, a powerful concept pioneered by Estrin and coworkers (13–16). In particular, Dyskin et al. (14) explored how regular, convex polyhedral (platonic) solids can interlock and serve as building blocks for TIMs, with examples including cubes (15, 17) and tetrahedra (18, 19). Nonplatonic geometries with planar surfaces such as truncated tetrahedra (20–22) or blocks with non-planar surfaces (8, 23–27) have also been proposed. Interestingly the interlocked blocks can still slide, rotate, or separate to some extent, providing a wealth of tunable deformation mechanisms and properties (12, 16, 28). For example, the frictional sliding of the blocks on one another can dissipate energy and confer TIMs with very high impact resistance compared with monolithic panels of the same materials, a strategy which can be used to overcome brittleness of glasses and ceramics. However, improvements in impact resistance and energy absorption are achieved at the expense of 40–80% losses in strength (11, 20, 25, 27, 29). Despite recent efforts in

unifying designs (30–32) and optimization (33, 34), there are still no comprehensive guidelines to select optimum architectures for given applications and requirements. In this work we systematically explored the design of architected panels based on platonic shapes and their truncated versions to gain insights into the structure–mechanics–performance relations of these systems.

Design and Fabrication of Architected Ceramic Panels

The base material we used in this study was calcium sulfate, a brittle mineral which can be shaped into complex geometries at room temperature. We choose a brittle material for the building blocks to highlight the capability of architecture to generate toughness from brittle components, and to avoid plastic deformations within individual blocks which can complicate the interpretation of the results (35). We used a replica casting technique to make a large number of calcium sulfate building blocks of high density (36). An array of building blocks was first 3D printed (Fig. 1 *A* and *B*) using a high-resolution digital light-processing printer (Micro HiRes model; EnvisionTEC). These blocks served as a positive shape to make a silicone mold (Fig. 1 *C* and *D*). A ceramic slurry (calcium sulfate powder + 19 wt % water) was then pressure cast into the mold (Fig. 1*E*), which produced ceramic building blocks with high density and homogeneity, uniform geometries, and smooth surfaces (see *Methods* for details). We reused the silicone mold several times to make many building blocks. The building blocks were then tape-transferred into a rigid aluminum frame to hold the blocks in place and to serve as an external ligament (Fig. 1*F*). The gap between the edges of the panel and the frame was filled with calcium sulfate paste which was cured before testing. This homogeneous region ensured a uniform transfer of

Significance

Topologically interlocked materials (TIMs) use frictional sliding to generate large deformations and build toughness in otherwise all brittle components. TIMs can be up to 10 times more impact resistant than their monolithic form, but this improvement usually comes at the expense of static strength. Here we report a TIM design based on octahedral blocks which is not only much tougher (50×) than monolithic plates of the same material, but also stronger (1.2×). With no evidence of upper bounds for strength and toughness, TIMs have a tremendous potential as high-performance structural materials. Based on our experiments we propose a nondimensional “interlocking parameter” which could guide the exploration of new TIM designs and other new architected systems.

Author contributions: M.M. and F.B. designed research; M.M. and T.Z. performed research; M.M., T.Z., and F.B. analyzed data; M.M. and F.B. prepared the figures; and M.M. and F.B. wrote the paper.

The authors declare no conflict of interest.

This article is a PNAS Direct Submission.

Published under the PNAS license.

¹To whom correspondence should be addressed. Email: francois.barthelat@mcgill.ca.

This article contains supporting information online at www.pnas.org/lookup/suppl/doi:10.1073/pnas.1807272115/-/DCSupplemental.

Published online August 23, 2018.

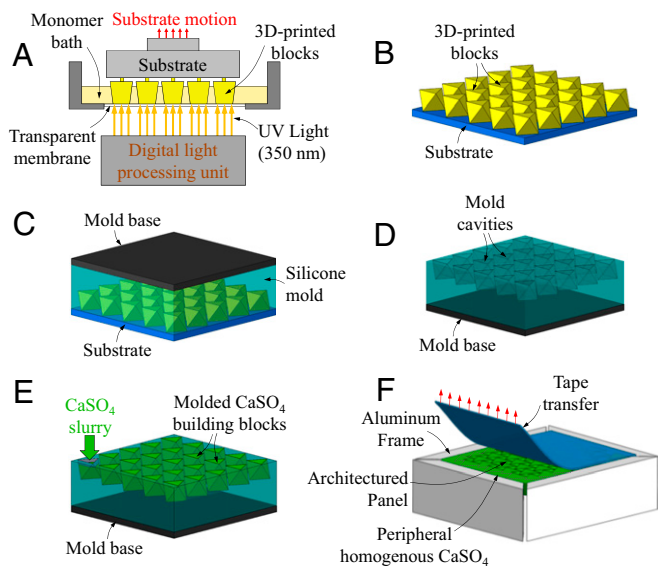


Fig. 1. Fabrication steps for the architected panels: (A) three-dimensional printing of polymeric building blocks; (B) the 3D printed blocks are transferred to a substrate; (C) silicone is poured to make a negative replica that serves as the mold; (D) the 3D printed blocks are removed from the cured silicone mold; (E) calcium sulfate (CaSO_4) is pressure cast into the silicone mold; (F) the building blocks are assembled and tape-transferred into an aluminum frame.

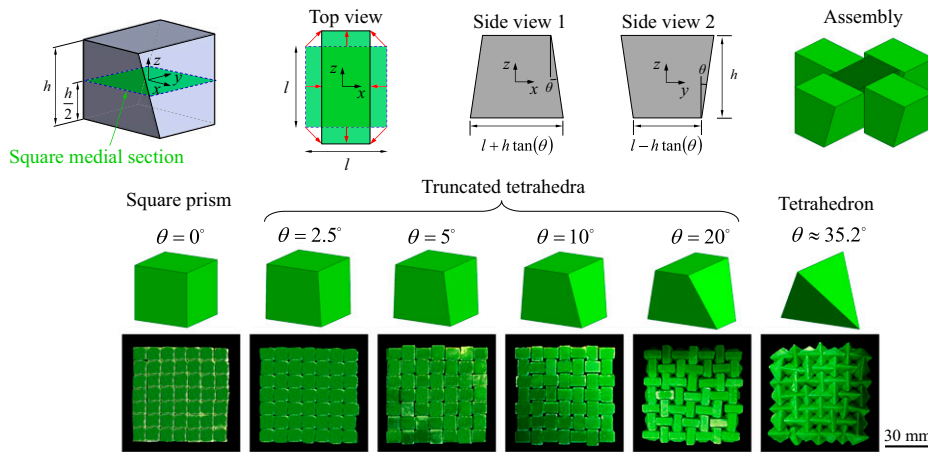
force from the frame to the peripheral blocks. We focused on convex polyhedral blocks, assembled into panels made of a 7×7 array of blocks. The number of blocks (and therefore their size) was fixed for all geometries to remove size effects (we recently showed that larger blocks lead to higher overall properties, *SI Appendix*, Fig. S1). Following the geometrical construction of Dyskin et al. (14), we required the medial sections of the blocks to form a surface-filling tessellation made of regular polygons (Fig. 2). There are only three regular shapes that can tile the plane: triangles, squares, and hexagons. We did not consider triangles as medial surfaces, because they cannot produce 3D interlocking geometries. Square medial section (Fig. 2A) was used to generate four flat faces that formed a prism capped with flat square faces at $z = \pm h/2$. The simplest geometry was a prism with dimensions $l \times l \times h$ which was assembled into panels held by friction only and without interlocking. The width of the medial square was set to $l = 5$ mm and the height was set to $h \approx 4.7$ mm. Interlocking geometries were introduced by tilting the opposed side faces of the prism inward by an angle θ , and by tilting the other pair of faces outward by the same angle θ . This procedure generated truncated tetrahedra (20) with geometries defined by three independent parameters: the medial section size l , the height of the block h , and the angle θ . In an architected panel, each block was geometrically constrained and interlocked by its four neighbors. Fig. 2A shows the effects of increasing θ from $\theta = 0^\circ$ to 2.5° , 5° , 10° , 20° up to $\theta \approx 35.2^\circ$, which corresponds to the limiting case of a tetrahedron. Increasing θ promotes interlocking, but also decreases the contact area between the blocks. In addition, for $\theta > 0$ the assembly leaves pyramidal empty space on the surface of the panel. To isolate and focus on the effects of geometry, we set $l = 5$ mm and adjusted h to maintain a constant areal density $\rho V/A = 1.09$ gr/cm^2 across all of the designs ($\rho = 2.3$ g/cm^3 is the mass density for calcium sulfate, V is the volume of an individual block, and A is the area of its medial section). Using the same approach, we also generated blocks based on hexagonal medial sections (Fig. 2B and C). These blocks were assembled into 7×7 panels with individual block size $a = 3.25$ mm, and the thickness h was adjusted to maintain the same areal density across all designs. The case $\theta = 0^\circ$ produced an eight-sided

prism with hexagonal base (Fig. 2B). Tilting of the side faces by alternating angles $(+\theta/-\theta)/+\theta/-\theta)/+\theta/-\theta)$ on the six side faces) produced truncated octahedra (Fig. 2B). The special case $\theta \approx 19.5^\circ$ corresponds to a regular octahedron, and further increase of θ produced truncated rhombohedra, up to the limit case of $\theta \approx 28^\circ$ corresponding to a full rhombohedron. Once assembled into panels, each block had six geometrically interlocked neighbors. Finally, a last case based on the hexagonal medial section is the regular dodecahedron, composed of 12 pentagonal faces. Because of the regular geometry of the dodecahedron, the interlocking angle is fixed at $\theta \approx 10.81^\circ$, and to keep the areal density constant we set $a' = 3.59$ mm (Fig. 2C). Our exploration therefore covered the first four of the five platonic shapes: tetrahedron, cube, octahedron, and dodecahedron; nonplatonic shapes such as the rhombohedron; as well as truncated versions of the octahedron, tetrahedron, and rhombohedron. In total, 15 building-block geometries were explored in this work. We did not consider the fifth platonic shape (icosahedron: 20 triangular faces), because none of its sections can tessellate a plane (14).

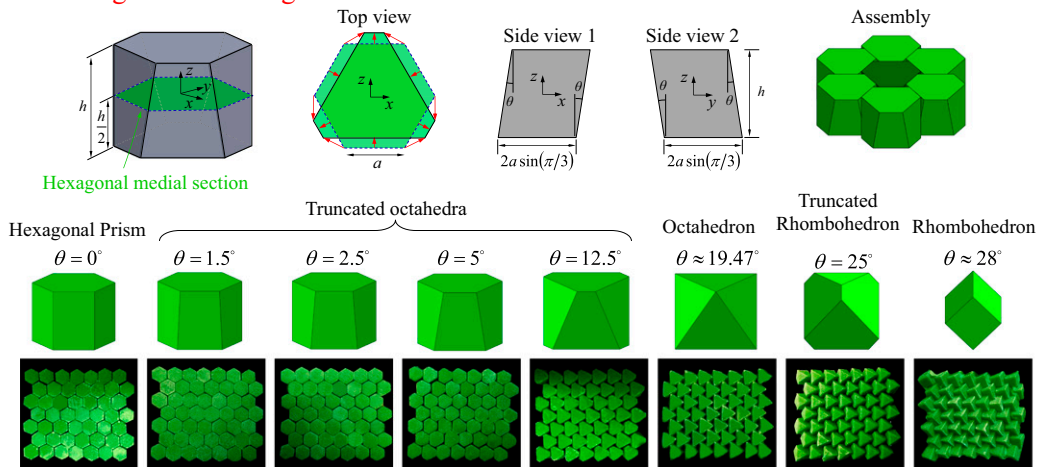
Mechanical Performance

The response of the panels to a transverse concentrated force was measured in quasi-static and impact loading conditions (Fig. 3A). The panel was simply supported and confined laterally by an aluminum frame. A localized force (or a 1-m/s impact) was applied on the top face of the center block. Fig. 3B shows the responses of an architected panel made of octahedral blocks in quasi-static and impact conditions together with the behavior of a monolithic calcium sulfate panel of the same areal density. As expected, the monolithic panel produced a linear elastic response immediately followed by a brittle failure at small deflections (~ 0.1 mm). Failure was catastrophic, with multiple cracks and fragmentation that extended to the edge of the panels (Fig. 3C). In contrast, the architected panel produced a bell-shaped response typical of tough materials. Compared with the monolithic panel the initial stiffness was in general lower, but the maximum deflection and the energy to failure were an order of magnitude greater. In addition, failure was localized with only the center block missing at the end of the test (Fig. 3C). We also used in situ stereovision, image correlation, and 3D scene reconstruction to measure the 3D displacements and rotations of the individual blocks during the tests (see *Methods* for details). The 3D reconstructed shape obtained from image correlation at six snapshots (points A–F in Fig. 3B) at various times during impact are shown in Fig. 3D. Typical results show that individual blocks rotate and slide on one another near the impact site (the deformation mode in quasi-static was identical). To characterize relative block motion for the entire plate, we computed the total sliding area at the interface and the average block rotation at different time points during the experiment. Taken together, these results point to a well-defined and repeatable deformation mode that follows two distinct stages (Fig. 3B): In the prepeak regime (region I), the average rotation and sliding area between the blocks rapidly increases with panel deflection. As the blocks slide on one another their contact area decreases, which is compensated by an increased geometrical locking so that an increasing force is produced. The slope of the force-deflection curve decreases gradually as the sliding increases, with fluctuations attributed to stick-slip mechanisms which are typical of dry friction (37). At the onset of transition from stage I to stage II, several sharp drops can be observed in the force-deflection curve due to surface cracking and chipping of individual blocks. The force however keeps increasing after each drop as the blocks reinterlock. In this example the maximum force (~ 180 N in quasi-static and ~ 190 N in impact) was achieved in this plateau-like region. In the postpeak region (stage II), sliding only occurs at the interface between the center block and its neighbors, so that the total sliding area increases more slowly with deflection. The average rotation of the blocks also

A Square-based tiling: Truncated tetrahedra



B Hexagon-based tiling: Truncated octahedra



C Dodecahedron

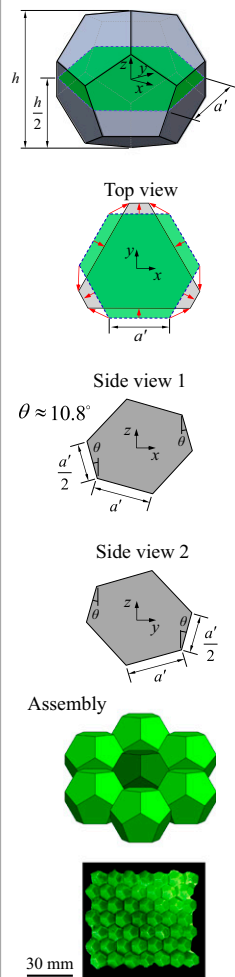


Fig. 2. Overview of the 15 architected panel designs explored in this study: For each group the geometry of the individual block is shown, together with a schematic of the assembly and pictures of 7×7 panels made of CaSO_4 blocks: (A) truncated tetrahedra based on a square medial section; (B) truncated octahedra based on a hexagonal medial section; and (C) dodecahedron.

decreases as the deformation of the panel partially recovers (Fig. 3B). The panel finally fails by complete push-out of the center blocks, in this case at a displacement $\sim 3\text{--}4.5$ mm. The failure is therefore localized, and the panel largely retains its shape and structural integrity, in contrast with the monolithic panel which failed catastrophically with multiple cracks (Fig. 3C).

The shape of the force-deflection curves and these mechanisms were similar for all of the panels (*SI Appendix, Figs. S2 and S3*). However, the performance of the panels in terms of stiffness, strength, and energy absorption (area under the force-deflection curve) varied across geometries. In general, the stiffness of the architected panel was about 50–75% lower than the monolithic panel (*SI Appendix, Fig. S4*). The strength was on the same order, but the energy absorption was far greater. All properties improved significantly with increasing interlocking angle, up to $\theta = 20^\circ$ (Fig. 4A–C). Stiffness tripled from $\theta = 0^\circ$ to $\theta = 20^\circ$, and maximum force and energy absorption increased by a factor of ~ 10 . These improvements in overall properties were generated by the increased interlocking between the blocks which restricted their relative motion. Interlocking angles higher than $\theta = 20^\circ$ however generated excessive contact stresses at the interfaces, which damaged individual blocks more extensively. In

particular, surface damage to the blocks decreased interlocking strength so that no further improvement was achieved for $\theta > 20^\circ$. The stiffness of the panel was similar in quasi-static and impact conditions, but the panels tested in impact produced higher maximum forces and energy absorption. We attributed these rate effects to four factors: (i) the monolithic ceramic was $\sim 10\%$ weaker (in terms of maximum force) in quasi-static loading compared with impact loading, which can be explained by sub-critical growth of flexural cracks in quasi-static loading, a well-documented effect in the failure of brittle materials (38). (ii) The sliding of the blocks is more extensive in impact loading (Fig. 3B). Indeed, previous studies showed that the static (39) and dynamic coefficients of friction (40) reduce significantly with the slip rate. This reduced coefficient of friction results in lower frictional stresses, which delays surface damage. In turn, delayed damage to individual blocks results in improved strength and in the spreading of sliding to more interfaces, resulting in improved energy absorption. We recently observed that reducing coefficient of friction improves performance in other types of interlocked architectures (35). (iii) The attenuation of elastic waves by the periodic architecture of the panels is another mechanism that can contribute to the improvement of energy absorption in impact (41).

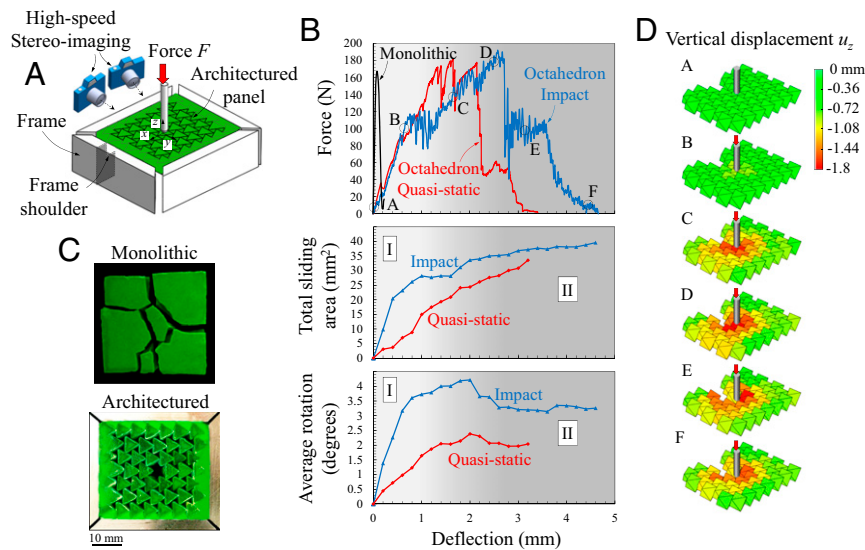


Fig. 3. Mechanical response of the architected panels. (A) Schematic of the experimental setup. (B) Force-deflection curves for architected panels made of octahedral blocks tested in quasi-static and impact conditions. The response of monolithic plate with the same areal density is also shown for comparison. The other two plots show the total sliding area and average rotation of the blocks over the course of the test obtained from stereoimaging and 3D reconstruction. (C) Postmortem samples: Monolithic plates fail catastrophically and by fragmentation, while in architected panels failure is localized to the central block. (D) Three-dimensional reconstruction of the panels showing the average vertical displacement of the blocks at six points (A–F) during loading.

Finally, (iv) the inertia resistance of individual building blocks may contribute to increased resistance to displacement in impact conditions (42). To estimate the inertia of the panel, we used the 3D reconstructed data to measure the velocity of each of the individual

blocks at the time of impact. The kinetic energy of each block was then computed and summed over the entire panel to obtain the total kinetic energy. The result, on the order of 3 mJ, was negligible in comparison with the total amount of energy dissipated in the

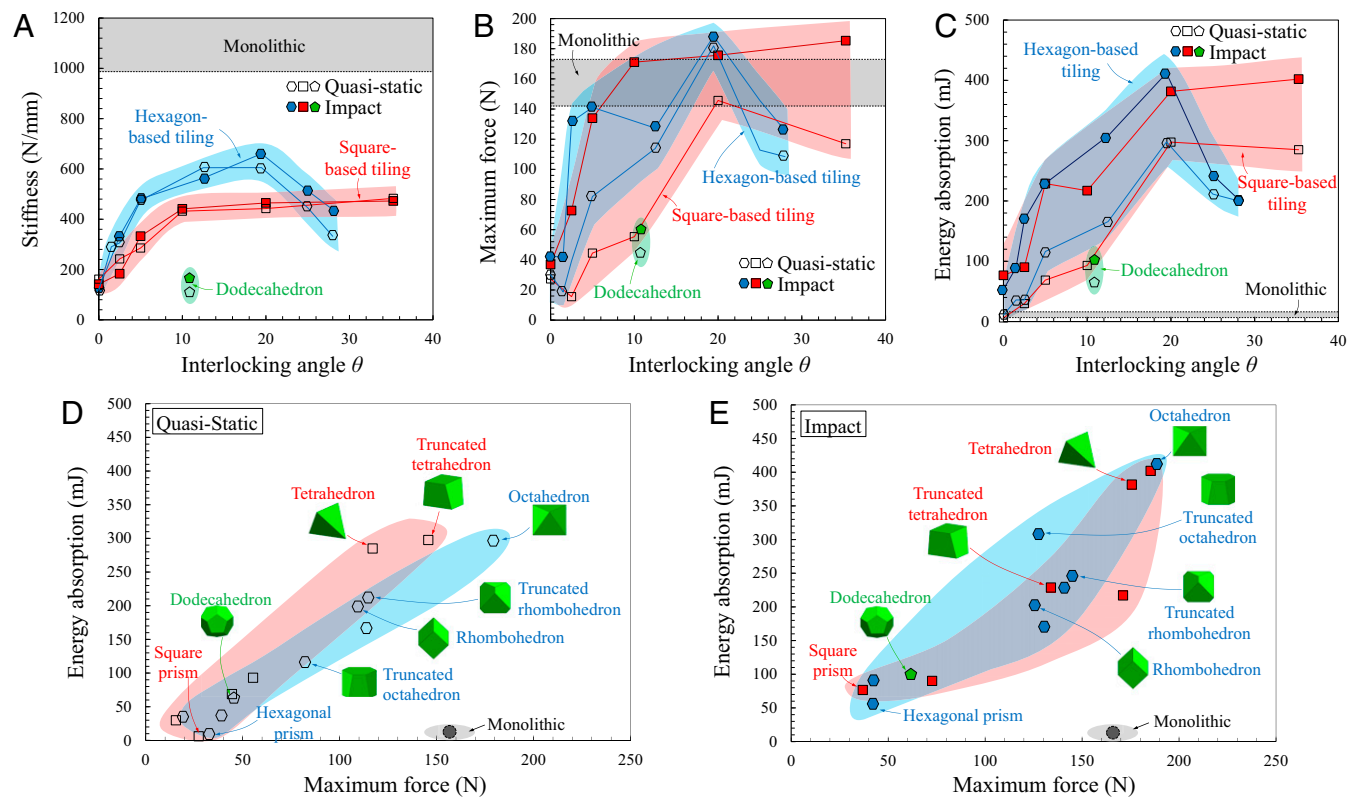


Fig. 4. Effects of architecture on the mechanical performance. Effect of interlocking angle on (A) stiffness, (B) maximum force, and (C) energy absorption; Maximum force-energy absorption chart and for all of the architected panels explored in this study tested in (D) quasi-static conditions and (E) impacts. The width of the colored regions is representative of the variations in the experimental results.

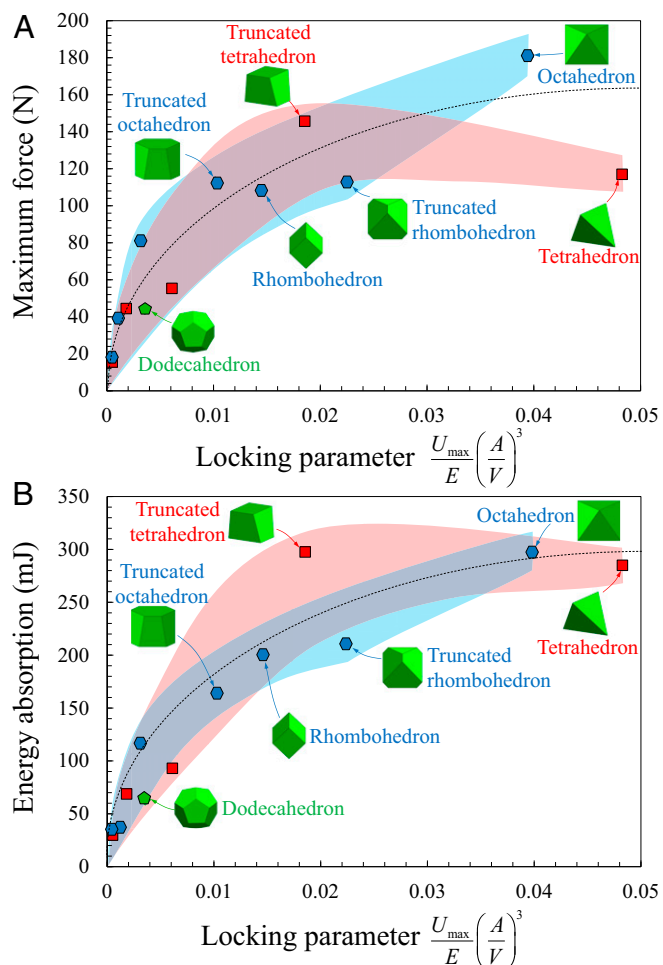


Fig. 5. A single nondimensional interlocking parameter, based on the strain energy stored in individual blocks during interlocking, can be used to predict (A) maximum force and (B) energy absorption. This approach may be effective in predicting the performance of other designs without the need for experiments or costly computational models. The width of the colored regions is representative of the variations in the experimental results.

panel (50–400 mJ). Microinertia therefore plays a negligible role in improving the performance of the panel in impact conditions.

The performance of the panels can be conveniently plotted in an Ashby chart that shows the energy absorption vs. strength in quasi-static (Fig. 4D) and impact (Fig. 4E) conditions. These charts highlight the superiority of the architected designs over the monolithic panels, and the positive effects of increasing the interlocking angle. Square-based and hexagon-based tiling showed similar performance, and in terms of combined strength and energy absorption, panels made of octahedral blocks showed the overall best performance in both quasi-static and impact conditions. The energy absorption for octahedral-block-based panels was $\sim 20\times$ and $\sim 25\times$ more than that of the monolithic panels in quasi-static and impact, respectively. When considering the actual energy dissipated by formation of cracks (see *Methods* for details of this analysis), the architected panels were 35–50 \times more energy absorbent than monolithic ones. In addition to dissipating more energy, octahedral-block-based panels were, respectively, $\sim 13\%$ and $\sim 18\%$ stronger in quasi-static and impact. To explain this unexpected and remarkable increase of strength, it is useful to consider the failure mode for the different panel designs. The failure of the monolithic panels was governed by flexural cracks, a detrimental mode of failure which creates long cracks and

ruins the load-carrying capability of the panel after the first impact (Fig. 3C). In contrast, flexural fracture was completely absent in the architected panels. The finite size of each block reduces their flexural span, so that compared with the monolithic plates the flexural stress in individual blocks is much smaller for the same applied force [we recently observed this strengthening effect for stiff plates of finite size supported by a compliant substrate (43)]. An alternate but equivalent explanation is given by considering that most critical flexural stresses occur in tension in the monolithic plate. In the architected plate these tension lines are disrupted by the interfaces between the blocks, which cannot carry tensile stresses. In addition to this effect, the distributed forces over three faces and an optimum locking angle increased the stability of individual blocks over long sliding distances.

The overall performance of the panels is governed by collective sliding mechanisms that involve geometry and frictional contact. Capturing these phenomena can be extremely costly computationally when multiple contacting elastic bodies are considered. Here we explored the possibility of capturing the geometrical effects using a single nondimensional number conveying the efficacy of the interlocking mechanism for any arbitrary design. Since the locking mechanism largely relies on elastic contact between the blocks, our model started by considering a single elastic block interlocked by rigid and stationary neighbors (*SI Appendix*, Fig. S5). We then considered a deformation mode where the center elastic block is pushed downward. The sliding between the blocks is considered frictionless but the geometrical interference between the sliding block and its rigid neighbors generates elastic deformations in the center block. In this simplified model, the elastic block represents the center block of the panel, which is subjected to a point force, and which undergoes large amounts of sliding but little rotation (at most 1.8° obtained from the 3D reconstruction results). We approximated the elastic energy U stored in the elastic block as a function of pushout distance (see *Methods* for details) and then we computed its maximum value U_{\max} for each geometry. We finally normalized the result to capture the effects of architecture only and to produce a nondimensional “locking parameter” $(U_{\max}/E)(A/V)^3$, where A is the surface area of the medial section of the block, V its volume, and E the elastic modulus of the solid material. Fig. 5 shows the strength and energy absorption as functions of the locking parameter for all of the designs tested in this study. Strength and energy absorption initially increase rapidly with the locking parameter, but the slope decreases progressively because of surface damage at the blocks due to contact stresses. These results suggest that the locking parameter could be used as a predictor of material performance for a wider range of designs and geometries, which could guide future explorations without the need for experiments or costly computational models.

Summary

In this study we have systematically explored topologically interlocked panels made of convex ceramic blocks. Under impact or transverse forces individual blocks slide and rotate, providing large deformations and toughness which leads to highly localized failure. In contrast, monolithic panels fracture in a brittle fashion and catastrophically by fragmentation. We have identified an architecture based on octahedral blocks which not only produces a 50-fold improvement in toughness compared with the monolithic form, but which is also $\sim 20\%$ stronger. The interfaces between the blocks cannot sustain tensile stresses and therefore disrupt tensile stresses which are the usual cause of failure in flexural panels. The octahedral design provides added stability because contact forces are distributed over three contact surfaces and because among the geometries explored here, this geometry provides the most efficient balance between interlocking strength and surface damage from frictional contact stresses. There is an infinite number of

other architectures to be explored, with some architectures which could lead to even higher performance (concave blocks, nonplanar faces). The exploration of this large design space is however difficult because experiments are lengthy and numerical models are computationally costly, if at all possible. To guide this exploration, we proposed a nondimensional interlocking parameter which we show correlates well with the performance of the panel. This parameter can be easily calculated for any geometry, which could greatly accelerate the exploration of new designs (a formal proof that the proposed interlocking parameter is a performance predictor for any arbitrary geometry remains to be established). The variability of our experimental results was similar for the monolithic and architected panels. However, it is not clear which type of distribution the strength of the TIM panels follows, because we do not have enough experiments for each configuration. The strength of the architected panels is partially governed by the onset of sliding between the blocks, which may follow a statistical law which is different from the weakest link (Weibull) statistics (44). More experiments and models are needed in this area, and questions related to statistics of failure for TIMs remain largely open.

An important design parameter for the architected panels is the coefficient of friction at the interfaces, which may be finely tuned by adding roughness on the surfaces of the blocks (24). Interestingly, nature is well ahead of engineers in making use of architected materials. Materials such as bone, teeth, or mollusc shells are also made of stiff building blocks of well-defined sizes

and shapes, bonded together by deformable bioadhesives. The remarkable mechanical performance of these materials (12, 45) can suggest new types of 3D architectures. In addition, the building blocks in natural materials do not simply interact through contact and friction, but also through complex polymers with sacrificial bonds, dynamic cross-links, and viscous behaviors (31, 46) which could also serve as inspiration for interfaces in synthetic architected materials. The segmentation of load-carrying structures into smaller elements joined by weaker interfaces is a counterintuitive approach to generate mechanical performance, but biological materials and recent studies on architected materials show that it is indeed a powerful strategy to overcome brittleness while retaining strength. New combinations of properties in these architected materials and systems can make them attractive for a variety of application including protective panels and armors, structural panels, or high-temperature structures.

Methods

Details of the derivation of the interlocking parameter (strain energy model) as well as experimental methods related to fabrication, testing, and data analysis can be found in [SI Appendix](#).

ACKNOWLEDGMENTS. This work was supported by Natural Sciences and Engineering Research Council of Canada and by the Fonds Québécois de la Recherche sur la Nature et les Technologies. T.Z. was partially supported by a Summer Undergraduate Research in Engineering Award from McGill University.

- Ashby MF (2005) Hybrids to fill holes in material property space. *Philos Mag* 85: 3235–3257.
- Brechet Y, Embury JD (2013) Architected materials: Expanding materials space. *Scr Mater* 68:1–3.
- Lakes R (1993) Advances in negative Poisson's ratio materials. *Adv Mater* 5:293–296.
- Berger JB, Wadley HN, McMeeking RM (2017) Mechanical metamaterials at the theoretical limit of isotropic elastic stiffness. *Nature* 543:533–537.
- Jaglinski T, Kochmann D, Stone D, Lakes RS (2007) Composite materials with viscoelastic stiffness greater than diamond. *Science* 315:620–622.
- Evans AG (1990) Perspective on the development of high-toughness ceramics. *J Am Ceram Soc* 73:187–206.
- Clegg WJ, Kendall K, Alford NM, Button TW, Birchall JD (1990) A simple way to make tough ceramics. *Nature* 347:455–457.
- Mirkhalaf M, Dastjerdi AK, Barthelat F (2014) Overcoming the brittleness of glass through bio-inspiration and micro-architecture. *Nat Commun* 5:3166.
- Bouville F, et al. (2014) Strong, tough and stiff bioinspired ceramics from brittle constituents. *Nat Mater* 13:508–514.
- Evans AG, Hutchinson JW, Ashby MF (1998) Multifunctionality of cellular metal systems. *Prog Mater Sci* 43:171–221.
- Siegmund T, Barthelat F, Cipra R, Habtour E, Riddick J (2016) Manufacture and mechanics of topologically interlocked material assemblies. *Appl Mech Rev* 68:040803.
- Barthelat F (2015) Architected materials in engineering and biology: Fabrication, structure, mechanics and performance. *Int Mater Rev* 60:413–430.
- Dyskin AV, Estrin Y, Kanel-Belov AJ, Pasternak E (2001) Toughening by fragmentation—How topology helps. *Adv Eng Mater* 3:885–888.
- Dyskin AY, Estrin Y, Kanel-Belov AJ, Pasternak E (2003) Topological interlocking of platonic solids: A way to new materials and structures. *Philos Mag Lett* 83:197–203.
- Estrin Y, et al. (2004) Negative stiffness of a layer with topologically interlocked elements. *Scr Mater* 50:291–294.
- Estrin Y, Dyskin AV, Pasternak E (2011) Topological interlocking as a material design concept. *Mater Sci Eng C* 31:1189–1194.
- Dugue M, Fivel M, Brechet Y, Dendievel R (2013) Indentation of interlocked assemblies: 3D discrete simulations and experiments. *Comput Mater Sci* 79:591–598.
- Khandelwal S, Siegmund T, Cipra RJ, Bolton JS (2012) Transverse loading of cellular topologically interlocked materials. *Int J Solids Struct* 49:2394–2403.
- Khandelwal S, Siegmund T, Cipra RJ, Bolton JS (2013) Scaling of the elastic behavior of two-dimensional topologically interlocked materials under transverse loading. *J Appl Mech* 81:031011–031019.
- Mirkhalaf M, Tanguay J, Barthelat F (2016) Carving 3D architectures within glass: Exploring new strategies to transform the mechanics and performance of materials. *Extreme Mech Lett* 7:104–113.
- Brocato M, Mondardini L (2012) A new type of stone dome based on Abeille's bond. *Int J Solids Struct* 49:1786–1801.
- Mirkhalaf M, Barthelat F (2015) A laser-engraved glass duplicating the structure, mechanics and performance of natural nacre. *Bioinspir Biomim* 10:026005.
- Autruffe A, et al. (2007) Indentation behaviour of interlocked structures made of ice: Influence of the friction coefficient. *Adv Eng Mater* 9:664–666.
- Djumas L, Simon GP, Estrin Y, Molotnikov A (2017) Deformation mechanics of non-planar topologically interlocked assemblies with structural hierarchy and varying geometry. *Sci Rep* 7:11844.
- Javan AR, Seifi H, Xu S, Ruan D, Xie Y (2017) The impact behaviour of plate-like assemblies made of new interlocking bricks: An experimental study. *Mater Des* 134: 361–373.
- Mirkhalaf M, Barthelat F (2017) Design, 3D printing and testing of architected materials with bistable interlocks. *Extreme Mech Lett* 11:1–7.
- Dyskin AV, Estrin Y, Pasternak E, Khor HC, Kanel-Belov AJ (2003) Fracture resistant structures based on topological interlocking with non-planar contacts. *Adv Eng Mater* 5:116–119.
- Brugger C, Bréchet Y, Fivel M (2008) Experiments and numerical simulations of interlocked materials. *Adv Mater Res* 47–50:125–128.
- Krause T, et al. (2012) Mechanical properties of topologically interlocked structures with elements produced by freeze gelation of ceramic slurries. *Adv Eng Mater* 14: 335–341.
- Naleway SE, Porter MM, McKittrick J, Meyers MA (2015) Structural design elements in biological materials: Application to bioinspiration. *Adv Mater* 27:5455–5476.
- Barthelat F, Yin Z, Buehler MJ (2016) Structure and mechanics of interfaces in biological materials. *Nat Rev Mater* 1:16007.
- Fratzl P, Kolednik O, Fischer FD, Dean MN (2016) The mechanics of tessellations—Bioinspired strategies for fracture resistance. *Chem Soc Rev* 45:252–267.
- Barthelat F (2014) Designing nacre-like materials for simultaneous stiffness, strength and toughness: Optimum materials, composition, microstructure and size. *J Mech Phys Solids* 73:22–37.
- Begley MR, et al. (2012) Micromechanical models to guide the development of synthetic 'brick and mortar' composites. *J Mech Phys Solids* 60:1545–1560.
- Malik I, Mirkhalaf M, Barthelat F (2017) Bio-inspired "jigsaw"-like interlocking sutures: Modeling, optimization, 3D printing and testing. *J Mech Phys Solids* 102: 224–238.
- Li J, Alati-Kut I, Hermansson L (1993) High-strength dental gypsum prepared by cold isostatic pressing. *Biomaterials* 14:1186–1187.
- Heslot F, Baumberger T, Perrin B, Caroli B, Caroli C (1994) Creep, stick-slip, and dry-friction dynamics: Experiments and a heuristic model. *Phys Rev E Stat Phys Plasmas Fluids Relat Interdiscip Topics* 49:4973–4988.
- Johnson HH, Paris PC (1968) Sub-critical flaw growth. *Eng Fract Mech* 1:3–45.
- Johannes V, Green M, Brockley C (1973) The role of the rate of application of the tangential force in determining the static friction coefficient. *Wear* 24:381–385.
- Di Toro G, et al. (2011) Fault lubrication during earthquakes. *Nature* 471:494–498.
- Davies B, et al. (2014) Hypothesis: Bones toughness arises from the suppression of elastic waves. *Sci Rep* 4:7538.
- Harrigan J, Reid S, Peng C (1999) Inertia effects in impact energy absorbing materials and structures. *Int J Impact Eng* 22:955–979.
- Chintapalli RK, Mirkhalaf M, Dastjerdi AK, Barthelat F (2014) Fabrication, testing and modeling of a new flexible armor inspired from natural fish scales and osteoderms. *Bioinspir Biomim* 9:036005.
- Rubinstein SM, Cohen G, Fineberg J (2004) Detachment fronts and the onset of dynamic friction. *Nature* 430:1005–1009.
- Wegst UGK, Bai H, Saiz E, Tomsia AP, Ritchie RO (2015) Bioinspired structural materials. *Nat Mater* 14:23–36.
- Dunlop JWC, Weinkamer R, Fratzl P (2011) Artful interfaces within biological materials. *Mater Today* 14:70–78.